Journal of Petroleum Exploration and Production Technology (2023) 13:219–235
https://doi.org/10.1007/s13202-022-01547-5

ORIGINAL PAPER-PRODUCTION ENGINEERING

Low-field NMR investigation on interaction of ZnO nanoparticles with reservoir fluids and sandstone rocks for enhanced oil recovery

Osamah Alomair[1] · Adel Elsharkawy[1] · Waleed Al-Bazzaz[2] · Salim Ok[2]

Received: 19 October 2021 / Accepted: 4 July 2022 / Published online: 20 July 2022

Abstract

The use of nanoparticles (NPs) can considerably benefit enhanced oil recovery (EOR) by changing the wettability of the rock, improving the mobility of the oil drop, and decreasing the interfacial tension (IFT) between oil and water. Prior to the application of nanoparticles in oil fields, it is essential to conduct measurements at the laboratory scale. However, the estimation of reservoir wettability is difficult in most laboratory experiments. Practicably, ZnO NPs were used to modify the rock surface wettability, lower the IFT at the oil/water interface, and reduce the interaction of chemical adsorption, such as (surfactant) onto reservoir rock surface to solve various challenges in oil production and EOR operations. Upon confining both ZnO-based nanofluid and the crude oil into sandstone, deviations from the corresponding pure bulk dynamical behaviors were observed with low-field nuclear magnetic resonance (LF-NMR) relaxometry. The expected deviations from the pure bulk behaviors were attributed to the well-known confinement effect. The wettability test results before and after surface variations of formation water (FW) with the addition of three different NP concentrations (0.05, 0.075, and 0.1) wt% ZnO reflected significant changes to its wettability. Among the treatments of Berea sandstone cores with ZnO NPs, the percentage of clay-bound H_2O/free fluid index was maximum in 1.0 pore volume (PV) NP treatment. The ratio of NMR relaxations, which determines the affinity of fluids toward solids, by the 1.0 PV NP treatment is reported to have the most potential with higher affinity for FW and less affinity for crude oil toward the pore walls. Hence, LF-NMR allows monitoring of nanofluid and crude oil characteristics in the pores of rock samples and may potentially be applied in further EOR studies.

Keywords Enhanced oil recovery · ZnO nanoparticles · Low-field NMR · Wettability alteration · Nanofluid treatment

Introduction

In the enhanced oil recovery (EOR) method, it is widely known that at least 60–70% of crude oil remains trapped as oil drops in pores in the discrete phase after primary and secondary recovery because of capillary forces (Brea et al. 2016). Since the demand for energy is increasing, the petroleum industry is investigating new methods to recover trapped crude oil where nanotechnology has shown promising results. The application of nanotechnology has been successful in some cases, including reservoir characterization (Rahmani et al. 2015) and drilling (Hoelscher et al. 2012).

For the oil and gas industry, different nanotechnology applications have been proposed based on laboratory experiments (Suleimanov et al. 2011; Zhang et al. 2014; Onyekonwu et al. 2010; Cheraghian et al. 2020; Udoh et al. 2021). Most of the reported results in the literature showed the potential of nanoparticles in improving oil recovery. Nevertheless, to the best of our knowledge, few field trials have been reported. The first reported attempt to utilize nanoparticles in a reservoir occurred in 2010, when Saudi Aramco performed a push–pull test using A-Dots (carbon-based fluorescent nanoparticles) in the Arab D formation of the Ghawar field. The results showed a high recovery percentage, up to 86%, suggesting their high stability (Kanj et al. 2011). Another trial was conducted in the same field and confirmed their high stability (Kosynkin and Alaskar 2016). In the Columbia oilfield, aluminum oxide and silica

✉ Osamah Alomair
dr.alomair@ku.edu.kw

[1] Petroleum Engineering Department, College of Engineering and Petroleum, Kuwait University, P.O. Box 5969, 13060 Safat, Kuwait

[2] Petroleum Research Center, Kuwait Institute for Scientific Research, P.O. Box 24885, 13109 Safat, Kuwait

NPs were used for the inhibition and remediation of formation damage. After 8 months of injecting aluminum oxide, the oil rate has increased by 300 bbl/d. Another trial using silica resulted in an oil and gas rate increase of 134 bbl/d and 1 MMSCF/d, respectively (Franco et al. 2017). Also in the Columbia oilfield, an unnamed nanofluid was used to enhancing the mobility ratio of heavy oils, and an immediate increase in the oil production rate was observed along with a reduction of 11% in the basic sediment and water production (Zabala et al. 2016) In Brazil, stabilizing a shale formation was achieved using a water-based drilling fluid containing nanoparticles. The results showed good performance in terms of shale hydration inhibition and wellbore stability. The same fluid was stored and used to drill another section in a different well after approximately 3 months and resulted in a 15% reduction in the well's cost (Barroso et al. 2018).

Due to their sizes ranging between 1 and 100 nm, the physical and chemical properties of NPs differ from their bulk behaviors (Suryanarayana et al. 1992 and Alsaba et al. 2020), and their unique properties allow them to have multiple impacts on the recovery of oil. NPs such as aluminum, iron, titanium dioxide, and silica were found to act as nano-catalysts which are highly beneficial to catalytic reactions during steam injection into heavy oil reservoirs due to their large surface-to-volume ratio, small size, and varied shapes (Hashemi et al. 2014). These nano-catalysts can be used to conduct upgrading in heavy oil reservoirs, converting bitumen to lighter products (Yoosuk et al. 2008; Almao 2012). These catalytic reactions fall under aqua-thermolysis which also include the breaking of carbon–sulfur bonds within asphaltenes, increasing saturates and aromatics in the heavy oil, which also has an impact on oil recovery (Hyne 1986).

Another path through which NPs affect oil recovery is their adsorption, which is a surface interaction that leads to the transfer of a molecule from a fluid bulk to a solid surface. This interaction mainly takes place between nano particles and rock surfaces. The major forces that can contribute to the adsorption process include electrostatic (Coulombic) interactions, charge transfer interactions, van der Waals interactions, repulsion or steric interactions, and hydrogen bonding (Cheraghian and Hendraningrat 2016; Olayiwol and Dejam 2019; Murgich 2002; Kokal et al. 1995). The main functions of NPs adsorption are to alter the rock wettability, lower the oil–water interfacial tension (IFT), and reduce chemical adsorption on the reservoir rock surfaces (Al-Anssari et al. 2016; Bera and Belhaj 2016; Hendraningrat et al. 2012; Ju et al. 2006; Kazemzadeh et al. 2019; Nowrouzi et al. 2019; Olayiwola and Dejam 2019; Saien et al. 2017; Zaid et al. 2013).

Wettability is a property of a fluid to cover a surface in the presence of other immiscible fluids (Van and Chon 2016). When oil and water are the immiscible fluids in oil reservoirs, the NPs strongly affect the rock surfaces wettability to reduce the oil–water IFT (Ali et al. 2018), which systematically influences the capillary pressure, permeability, and flow behaviors of fluids in the rock pores (Khalil et al. 2017). During their injection into rock pore spaces, NPs have been shown to arrange themselves in the oil–water–rock system as a well-structured wedge film between the surface of the rock and the oil, exerting a disjoining pressure on the film and separating oil from the surfaces of the rock (Azizr et al. 2018; Khalilnezhad et al. 2019; Kondiparty et al. 2011).

One of the most favorable NPs is zinc oxide (ZnO), which has a high surface charge and can function as a surface-active agent to replace surfactants (Soleimani et al. 2016). The small size of the NPs allows penetration of smaller pores to mobilize the capillary-trapped oil (Yahya et al. 2014). The adsorption of NPs on rock surfaces in oil reservoirs can modify the wettability condition from oil wet to water wet (Gurgel et al. 2008; Lianga et al. 2019) with the formation of an interface between the oil and water surfaces. Rezk and Allam (2019) reported an increase of about 8% of oil-recovery efficiency when both ZnO NPs and a surfactant mixture were employed when compared to a surfactant-based oil-recovery process in the case of sandstone.

However, NPs also have their limitations. For example, their release into the aquatic ecosystems through industrial wastewaters can induce pernicious effects on fish and other organisms, increasing concerns of environmental hazards. Several characteristics of ZnO NPs (e.g., size, shape, surface charge and agglomeration state) play a central role in biological effects such as genotoxic, mutagenic, or cytotoxic effects. Further, ZnO NPs may interact with the bacterial surface and/or with the bacterial core, exhibiting different bactericidal mechanisms (Jiang et al. 2009). Furthermore, economic feasibility is the major drawbacks when employing nanoparticles (NPs) in the petroleum industry (Bera and Belhaj 2016). Consequently, it has become necessary to investigate applications of nanotechnology within a laboratory environment, especially before applying NPs in the field.

Low-field nuclear magnetic resonance (LF-NMR) relaxometry techniques were developed in the laboratory to enhance and support comparable NMR logging tools that are currently used downhole. LF-NMR relaxometry has shown that discrimination of water and oil saturation in core and raw material can be easily determined. In such cases, the NMR can detect the total water weight fraction and the total oil weight fraction, the viscosity of the oil, the amount of bound or mobile water and the amount of mobile or bound oil (Mirotchnik et al. 1998; Mirotchnik and Kantzas 1999).

Additionally, LF-NMR has been applied in the crude oil industry because of its high potential to determine fluid and rock properties (Barbosa et al. 2015; Hou et al. 2020; Ok and Mal 2019) using both in situ and ex situ methods. LF-NMR has several advantages such as being non-destructive,

fast, reliable, and easy-to-operate (Barbosa et al. 2013; Jiang et al. 2021). LF-NMR provides time-domain relaxation data. In a typical NMR relaxation measurement, the relaxation processes reinstate the equilibrium magnetization after excitation of the spin ensemble (Ridwan et al. 2020). Longitudinal (T_1) and transverse (T_2) NMR relaxation times explain magnetization vector components that are parallel and perpendicular to the external magnetic field (B_0), respectively. The T_1 and T_2 values of molecules depend on fluctuations of the NMR interactions due to molecular motions. Hence, T_1 and T_2 measurements have become conventional techniques to explore molecular reorientations both in pure bulk state and in confined geometries (Abragam 1961; Gautam et al. 2017; Vogel 2010). LF-NMR measurements of fluids confined into rocks can be utilized to predict several petrophysical properties including porosity, pore size distribution, and free fluid index (Connolly et al. 2019).

In wettability measurements, nuclear magnetic resonance (NMR) interrogates the character of water molecules which changes based on whether the water molecules are in contact with rock or in the liquid phase. Borysenko et al. (2009) demonstrated that NMR determination of wettability showed a good correspondence with contact angle measurements. Odusina et al. (2011) used NMR to examine shale wettability, and Sulucarnain et al. (2012) studied shale wettability and effective surface relaxivity. NMR offers advantages such as being less expensive and faster than the USBM or Amott methods for single measurements. NMR can also monitor wettability changes, and the results can also be compared with normal geophysical logs that directly interrogate the reservoir in a continuous manner.

The goal of this study is to assess the potential of ZnO NPs in EOR processes with the aid of LF-NMR, to reduce IFT and alter wettability in the confined geometries and nanopores of sandstone rock samples, where oil and water molecules show strong deviations from their bulk behaviors. To achieve this goal, ZnO NPs were first thoroughly characterized by elemental composition analysis and surface area determination. Then, blends of formation water (FW) and crude oil were studied in bulk using various approaches, including IFT tests and water contact angle measurements. Finally, the non-destructive and reliable LF-NMR technique was applied to evaluate sandstone samples saturated with oil and nanofluid.

From a practical viewpoint, this study will be valuable in EOR for developing a new high-precision LF-NMR approach, which is faster and more reliable in measuring or estimating rock wettability through different chemical conditions present in the oil fields. This method will be an alternative to methods of Amott-Harvey, USBM (US Bureau of Mines test), (sessile drop) methods used in the laboratory and reservoir, Anderson (1986), and Abdallah et al. (2007). The novelty of the work lies in the fact that the wettability of the rock surface affects the distribution of fluids within the pore space, and the oil and water distribution can be obtained by comparing the NMR relaxation data at different saturations (Al Harbi et al. 2017). Also, accessible advance integrated petrophysical evaluation for in situ wettability to support the field development and improve the reservoir characterization.

Experimental details

Materials and properties

Core samples

Synthetic Berea Sandstone core plugs were purchased from Kocurek Industries Inc. (Houston, TX, USA). The core samples were cleaned using distillation–extraction Soxhlet apparatus with a 50/50 mixture of toluene/methanol and subsequently dried in a vacuum oven at 80 °C (1CE, Thermo-Fisher Scientific with Hydraulic Thermostat Controller, UK). The porosity and permeability of the core test samples were measured using Helium PHI-220 Porosimeter and KA-210 Gas Permeameter, respectively. Both instruments were supplied by Coretest Systems, Inc., USA. The porosities at pressure and temperature (400 psia, 25 °C) and for permeabilities (250 psia, 25 °C) were measured at a confinement pressure 500 psia as recommended by the manufactures. The core properties are shown in Table 1. The average element analysis using (EDXRF, Epsilon-1 Malvern analytical Ltd UK) are presented in Table 2, and X-ray diffractometer (XRD) analysis, using D8 Advance Bruker GmbH, was performed to reveal the amount of different crystals existing in the Berea Sandstone specimens as shown in Fig. 1. Formation water (FW)

FW of low salinity and low conductivity was employed in this study. The conductivity, total dissolved solids (TDS), and salinity of the FW (30,000 ppm) were measured using a VWR traceable hand-held meter (Chemicals and Laboratory Scientific Company), while the turbidity was measured using a HACH model 2100P portable turbidimeter (GmbH, Germany). The detailed physicochemical properties of the FW are summarized in Table 3. Besides, the distribution of the solid particles in the FW was determined using dynamic light scattering (DLS) by a Zetasizer Nano ZS-ZEN3600, DLS, USA. The average particle diameter was 1760 nm after filtration with sterile poly-ether sulfone (PES) syringe filters with four layers, followed by a membrane filter, resulting in average particle size of 380 nm.

The particle size distribution of FW averaged at 1250 nm, obtained by DLS (Fig. 2). In addition, the rock heterogeneity was qualitatively observed from the frequency graph of the pore throat diameter (Fig. 3). The fraction of pores

Table 1 Dimensions and petrophysical properties of the core samples

Serial	Length (cm)	Diameter (cm)	Bulk volume (cm^3)	Pore volume, PV (cm^3)	Lithology	Porosity (%)	Air permeability (md)
S0	7.42	3.78	83.226	15.724	Sandstone	18.9	125
S1	7.65	3.78	85.805	15.985		18.6	124
S2	7.36	3.78	82.553	15.206		18.4	138
S3	7.38	3.78	82.777	15.501		18.7	120
S4	7.57	3.78	84.908	15.529		18.3	120
S5	7.49	3.78	84.011	15.235		18.1	138
S6	7.51	3.78	84.235	15.735		18.7	144

Table 2 Elemental analysis of Berea sandstone

Chemical Formula	Quantity (wt%)
SiO_2	88.44
Al_2O_3	4.55
Fe_2O_3	1.31
K_2O	1.112
Na2O	0.341
SO_3	0.202
CaO	0.311
Mn_3O_4	0.037
ZrO_2	0.036
P_2O_5	0.018
SrO	0.005
ZnO	0.002
PbO	0.003
SrO	0.004

(y-axis) was calculated as the volume of injected mercury divided by the pore volume of the core sample. The pore size distribution of Berea sandstone is normal with a relatively narrow peak less than those suggested by Gong et al. (2020). Thus, the FW is considered suitable for the present study because the particle size distribution is less than the pore size distribution. The rock heterogeneity might be also qualitatively observed from the frequency graph of the pore size distribution.

Crude oil

Samples of crude oil were collected from a Kuwaiti oilfield; the field produces medium to light crude oil with an API gravity of 28–36°. The samples were stored in specially designed screw-cap bottles under dry conditions in a thermostatic fume hood at 25 °C. The basic sediments and water (BS&W) were determined using the ASTM D4007-11. The density was measured at 25 °C using a precision digital Anton Paar oscillating U-tube densitometer, DMA4500, with a reproducibility of 10^{-2} kg m^3. The dynamic viscosities were also measured as a function of temperature (20, 25, 30, and 40 °C) using an SVM 3000 Stabinger Anton Paar viscometer. SARA Analysis (saturates, aromatics, resins, and asphaltenes) was done using IATROSCAN MK-6s (Mitsubishi Chemical Medience, Japan). The physical properties of the crude oil are tabulated in Table 4.

Zinc oxide (ZnO) nanoparticle (NP)

ZnO NP was purchased from Skyspring Nanomaterials Inc, USA, without any additional treatment. The properties of ZnO NP shown in Table 5 were investigated experimentally using an automatic absorptiometry surface area analyzer (ASAP-2010, Micrometrics USA).

Methodology

Stability, dispersion, and adsorption of the ZnO NP

Particle stabilization is important for preventing particle agglomeration and formation damage. To represent real operating conditions, known masses of all the NPs of ZnO at three concentrations of (0.05, 0.075, 0.1) wt% were mixed with FW (30,000 ppm) and stirred continuously for 3 h using a digital stirring plate (Thermo Scientific, USA) at 500 rpm, with overnight storage in an oven at 30 °C. A cloudy solution was observed in all samples. To avoid high dispersion of NPs in the solution and reduce or prevent the possibility of particle agglomeration, each prepared solution was subjected to ultrasonication for 60 min using a Hielscher ultrasonic mixer (model UP200s, GmbH), as proposed by Chung et al. (2009) and Graves et al. (2019). Moreover, to evaluate the dispersion stability of nanofluids, the zeta potential (ξ-potential) was measured and calculated using the Helmholtz–Smoluchowski equation (Wilson et al. 2001; Munson et. al. 1998).

In the Brunauer–Emmett–Teller (BET) method of surface area analysis (Brunauer et al. 1938), liquid nitrogen is

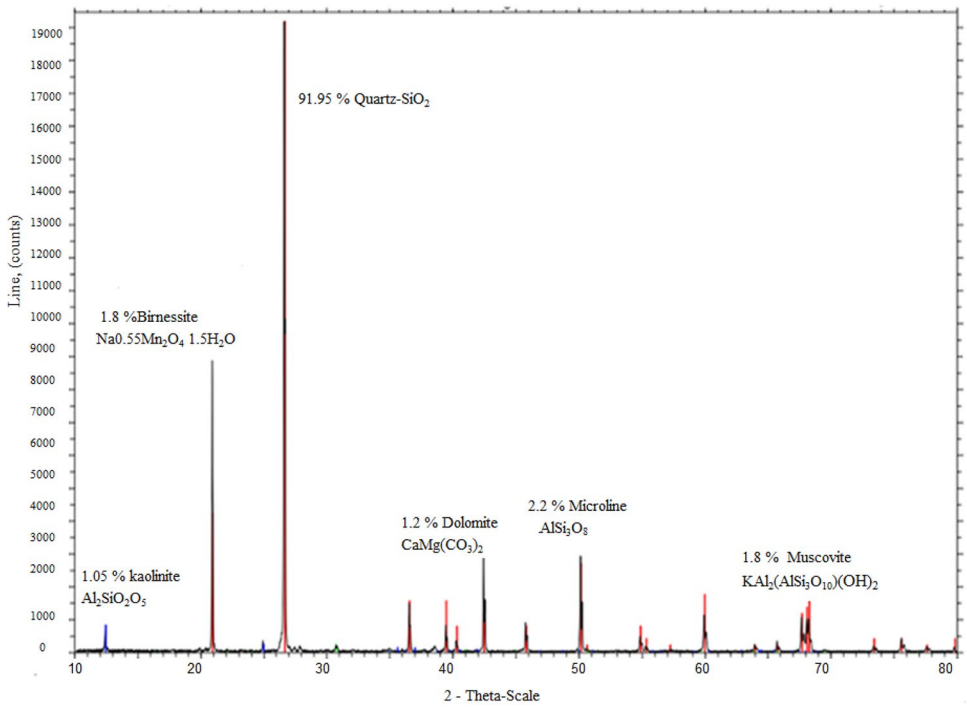

Fig. 1 XRD of the dry Berea sandstone core

Table 3 Properties of the FW

Designation	Concentration	Units
Salinity	30,000	mg l^{-1}
Total suspended solid (TSS)	2.400	mg l^{-1}
Turbidity	0.430	NTU
pH	6.030	@ 25 °C
Conductivity	46.000	(mS cm^{-1}) @ 25 °C
Strontium	75.150	mg l^{-1}
Boron	48.066	mg l^{-1}
Barium	3.792	mg l^{-1}
Lithium	7.634	mg l^{-1}
Silicon	14.893	mg l^{-1}
Nitrate (as NO_3)	0.000	mg l^{-1}
$MgCl_2{\cdot}6H_2O$	55.790	mg l^{-1}
$CaCl_2{\cdot}2H_2O$	143.816	mg l^{-1}
$BaCl_2{\cdot}2H_2O$	0.014	mg l^{-1}
$SrCl_2{\cdot}6H_2O$	3.302	mg l^{-1}
Na_2SO_4	0.887	mg l^{-1}

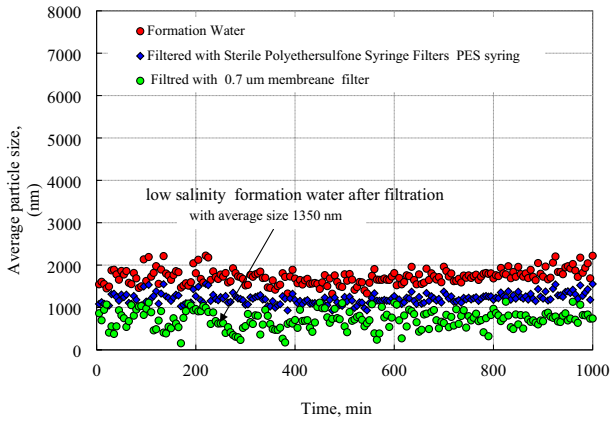

Fig. 2 DLS results of FW

usually used at partial vacuum conditions to cool surfaces and detect adsorption since the interaction between gaseous and solid phases is generally weak. N_2 (− 195 °C) gas used was a 99.999% pure product of Kuwait Oxygen and Acetylene Company KOAC (Kuwait). The specific surface areas (S_{BET}) were calculated from the BET equation in its linear form (Brunauer et al. 1938) with the nitrogen molecule cross-sectional area taken to be 16.2×10^{-20} m^2 (linearity region between 0 and 0.35 p/p_0). The total pore volume was estimated from a single point on adsorption isotherm at p/p_0/0.975 (Badalyan et al. 2003 and Brundle et al. 1992). The pore size distributions were calculated in the standard manner using the Barrett–Joyner–Halenda (BJH) method (Barrett et al. 1951), and the pore size analyses done as stated by Siegbahn et al. (1967) are shown in Table 4.

IFT and contact angle measurements

The main purpose of these measurements is to evaluate the effect of ZnO NP on IFT and contact angle and to subsequently determine the optimum concentration of NP using NMR. The IFT for the oil/FW and oil/nanofluid systems was characterized, using a drop shape analyzer (DSA 100, Kruss,

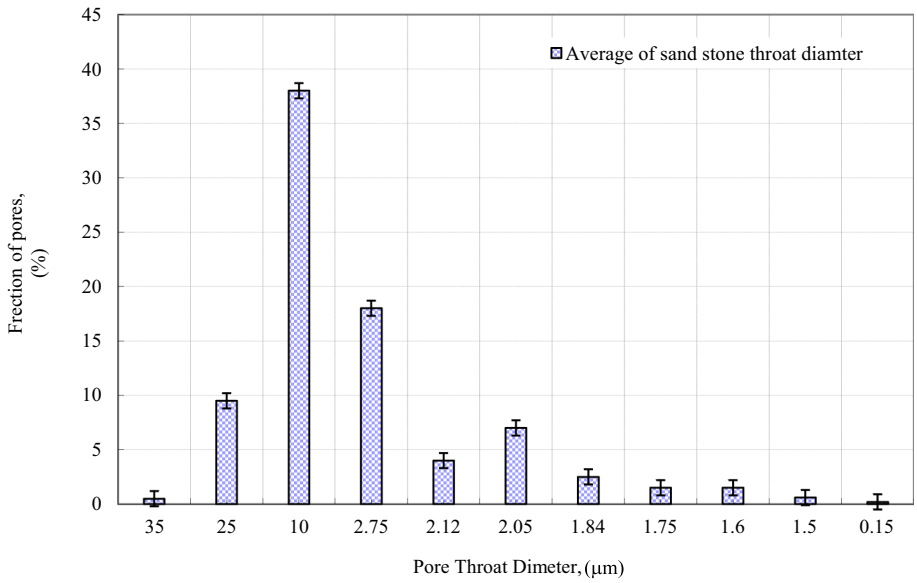

Fig. 3 Pore throat diameter distribution of Berea sandstone

Table 4 Physical properties of dry crude oil samples

Sample	Units
Water content at 2500 rpm	5 mL
Sediment	0.025 mL
Crude oil assay	
Dynamic viscosity @ 20 °C	41.7 mPa s
Dynamic viscosity @ 25 °C	30.0 mPa s
Dynamic viscosity @ 30 °C	21.7 mPa s
Dynamic viscosity @ 40 °C	10.6 mPa s
Density @ 25 °C	0.8915 g cm^{-3}
SARA test	
Saturate (*S*)	9.10%
Aromatic (*A*)	68.93%
Resin (*R*)	13.17%
Asphaltene (As)	8.80%

GmbH), based on the pendant drop method (Ayatollahi and Zerafat 2012). The contact angles between the fluids under study and the selected Berea Sandstone were determined, and the wettability was identified according to the criteria (Teklu et al. 2015).

The apparatus was calibrated according to manufacturer recommendations with the standards provided; these standards consist of glass slides with modeled drop shapes, which are accurately calculated. Glass slides were used to calibrate the apparatus using the Young–Laplace method. Shapes with contact angles of 30°, 60°, and 120° each for standard and microscope optics deviated by less than 0.1° from their nominal values. The sessile drop was used for preferential determination of wettability test used in core flooding tests for measuring the contact angle directly. The flooded cores were cut in slices and prepared following the same method proposed by Ayatollahi and Zerafat (2012), and the drop of the nanofluid was introduced at the surface. The DSA-100 apparatus equipped with a high-resolution camera and digital processing software was used to perform contact angle measurements, and the results of measurements were checked for repeatability at least three times for each experiment. Finally, the results were averaged.

Fluid displacement experiments

Fluid displacement experiments were carried out in the core flooding system shown in Fig. 4. The system was mainly used to prepare the core plugs needed to conduct the NMR experiments based on the optimum results originated from IFT and contact angle. Besides the dry core sample (*S*0), which was used as reference for NMR, the following six samples were prepared: (*S*1) 100% saturation with FW; three pore volumes of FW were injected in the clean dry rock sample followed by soaking the core in FW at a rate of 0.5 cm^{-3} min^{-1} for about 1 h to ensure complete saturation. (*S*2): 100% saturation with crude oil; three pore volumes of crude oil were injected in the clean dry rock sample; then the core was infused with the crude oil at the rate of 0.5 cm^{-3} min^{-1} for about 1 h to ensure complete saturation. (*S*3–*S*6): rock restoration and nanofluid injection; the remaining rock samples were restored to represent reservoir saturation profile; initially flooded with FW until reaching 100%; in the next step, oil sample was injected at a rate of 0.5 cm^{-3} min^{-1} until no more water was removed; then nanofluid was injected with a specified concentration and required pore volumes.

Table 5 Physicochemical properties of ZnO NPs

Designation	Units
Purity	99.80%
Average particle size, (APS)	10–50 nm
Thermal conductivity	21 W m^{-1} K^{-1}
Surface area	
Single point surface area at $P/P_o = 0.236288865$	22.5774 m^2 g^{-1}
BET surface area	22.9994 m^2 g^{-1}
t-plot external surface area	21.7274 m^2 g^{-1}
Barrett–Joyner–Halenda (BJH) adsorption cumulative surface area of pores between 1.7 and 300 nm width	23.9910 m^2 g^{-1}
Pore volume	
BJH adsorption cumulative volume of pores between 1.70 and 300.0 nm width	0.098833 cm^3 g^{-1}
Single point adsorption total pore volume of pores less than 459.0618 nm width at $P/P_o = 0.995788234$	0.098679 cm^3 g^{-1}
Pore size	
Adsorption average pore width (4 V/A by BET)	17.16205 nm
BJH adsorption average pore width (4 V/A)	16.4779 nm
Horvath–Kawazoe maximum pore volume at $P/P_o = 0.844589971$	0.025370 cm^3 g^{-1}
Median pore width	3.7483 nm

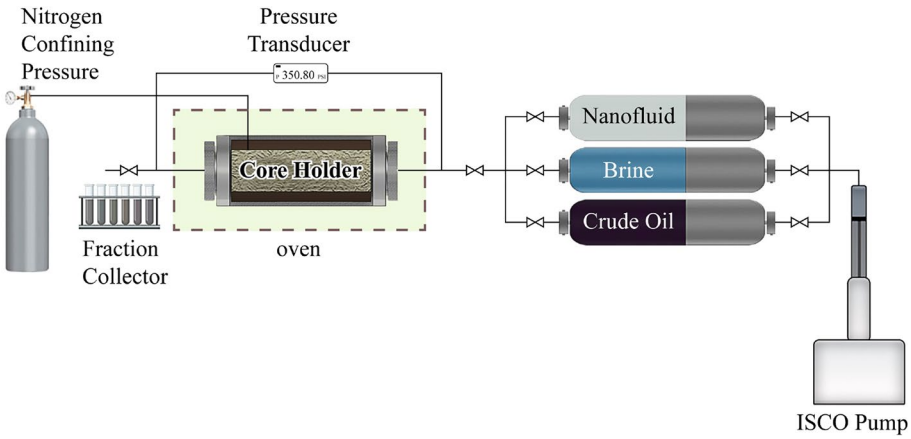

Fig. 4 Flow diagram of core saturation and flooding equipment

LF-NMR relaxometry details

The LF-NMR relaxometry data of the rock core samples were obtained on a 2.35 MHz Oxford GeoSpec2 Instrument, UK, with a 43-mm-diameter probe using the software Lithometrix 8.5.0. In flooded sandstone rock cores, the duration of the 90° pulse was 9.5 µs. To obtain T_2 data, the Carr–Purcell–Meiboom–Gill (CPMG) pulse sequence was used with a recycle delay time of 1125 ms, while an inversion recovery pulse sequence with a 3000 ms recycle delay time was used for the T_1 data. The number of detected points (spin echoes) in the T_2-pulse sequence was varied within the range from 32,401 to 4630 depending on the sample, and 12,963 was for oil and 115,741 for water. Three-exponential fitting analysis of T_1 relaxation data was performed according to the following equation:

$$y(x) = \sum_{i=1}^{3} A_i exp\left(\frac{x}{T_{1(i)}}\right) \quad (1)$$

where x stands for the signal detection time and $T_{1(i)}$ is the longitudinal relaxation time of the i-th component with respective amplitude A_i. A three-exponential fitting analysis of the T_2 relaxation data was then performed according to the following equation:

$$y(x) = \sum_{i=1}^{3} A_i \exp\left(-\frac{x}{T_{2(i)}}\right) \quad (2)$$

where x stands for the signal detection time and $T_{2(i)}$ is the transverse relaxation time of the i-th component with respective amplitude A_i (Aursand et al. 2008; D'Agostino et al. 2012). The three-component fitting gives the freedom of

determination of differing fractions, either heavy or light, of the crude oil in bulk and assigns the confined fluids inside such pores with different porosities.

Considering bulk crude oil, we suggest that the shortest T_2 value ($T_2(1)$) is attributed to the heaviest components, asphaltenes and resins, while the longest T_2 value ($T_2(3)$) to saturated aliphatic chains, where $T_2(2)$ values belong to aromatics; referring to A_1, A_2, and A_3 values, it is possible to suggest the percentages of crude oil fractions. In the confined fluids, three-component fitting is preferred to describe how the two fluids are distributed in the pores with various sizes.

The continuous distributions of T_1 were obtained from T_1-inversion recovery relaxation using the CONTIN algorithm (Provencher 1982). The permeability and porosity were determined using the following equation for T_1 distributions (Alvarado et al. 2003; Kenyon and Kolleeny 1995; Aghda et al. 2018):

$$k = \phi^4 * T_1^2\left(k = \frac{\phi}{C}\right)^4 * \left(\frac{\mathrm{FFI}}{\mathrm{BVI}}\right)^2 \quad (3)$$

where k is the permeability (millidarcy: md), T_1 is the longitudinal relaxation time (s), ϕ is the fractional porosity ($m^3\ m^{-3}$), C is an empirical coefficient ($md^{-0.25}$), BVI is the bound water volume index, and FFI is the free fluid index.

For processing the T_1 distribution data of sandstone cores using Eq. 3, the default value of 10 was employed for C (Coates coefficient: p.u./$md^{1/4}$) (Trevizan et al. 2015). T_1 distributions were utilized in the present study to estimate both the volume of producible fluid (Straley et al. 1991) and to show potential wettability alterations in sandstone rocks with certain porosities because T_1 distributions are reflections of porous media saturated with different fluids: low viscous FW versus highly viscous crude oil (Giraldo et al. 2013; Dang et al. 2013). The NMR estimate of a product is most often considered as the free fluid index (Straley et al. 1994).

Results and discussion

Stability, dispersion, and adsorption of ZnO NP

It was concluded that the stability of nanofluid depends on the pH, NP size, NP type (hydrophilic, hydrophobic, and amphiphilic), dispersion fluid, and ultrasonication time. The stability of dispersions is their long-term integrity and ability to remain in their initially formulated state by remaining as close as possible to their initial physical state. Because complex formulations are unstable by nature, the apparent dispersion stability can only be evaluated when the dispersed phase remains suspended, as stated by Tso et al (2010). The particle size distribution of ZnO nanofluid is shown in Fig. 5.

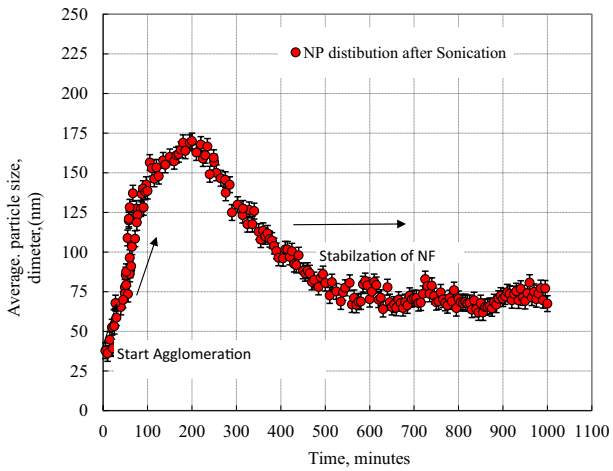

Fig. 5 Average particle size distribution of ZnO in FW after sonication

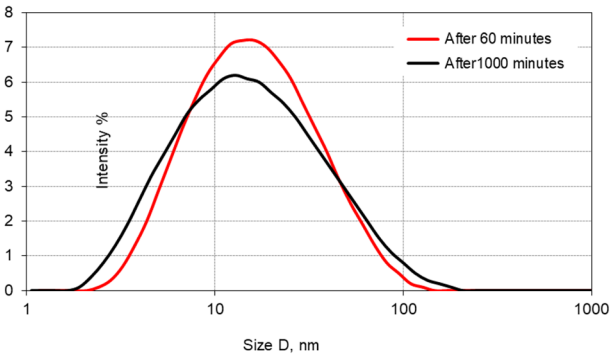

Fig. 6 Non-negative least square method shows the dispersion of ZnO NP in formation water at 60 and 1000 min

The zeta potential is a key indicator of the stability of a colloidal dispersion. The measured ξ-potential values of the ZnO nanofluid of concentration (0.05, 0.075, and 0.1) wt% were − 28.8, − 29.8, and − 29.1, respectively, with an average value of − 29.23, indicating a certain degree of electrostatic repulsion between adjacent similarly charged particles. Colloids with high zeta potentials (negative or positive) are electrically stabilized. A value of ± 25 mV can thus be taken as the arbitrary threshold that differentiates low-charge surfaces from highly charged surfaces (Dukhin and Goetz 2010).

The dispersion of ZnO NP in FW was measured using DLS based on the non-negative least-square algorithm method (Lawson and Hanson 1974). This suggested that using the ultrasonic processor during nanofluid preparation might break down the agglomeration of NPs and improve their dispersion. Figure 6 shows the normal distributions using the algorithm method to reconstruct particle

size distribution (PSD) from DLS data at 60 and 1000 min indicating the stability of the dispersion with time.

The ability of ZnO for adsorption built on BET isotherm model was investigated by plotting the amount of gas adsorbed as a function of the relative pressure (Gomez-Serrano et al. 2001; Maa et al. 2019). The adsorption type is (Type II). This is most frequently found when adsorption occurs on nonporous powders or powders with diameters exceeding micropores and the Inflection point occurs near the completion of the first adsorbed monolayer. Figure 7 shows the relationship between relative pressure (P/P_o) and ZnO adsorption capacity measured by quantity adsorbed (Q) = 62.79 $cm^3\ g^{-1}$ STP. Indeed, the conventional methods such as BET and BJH models cannot distinguish between different pore structure morphologies to account for the effects of microporosity and predict the pore sizes that could

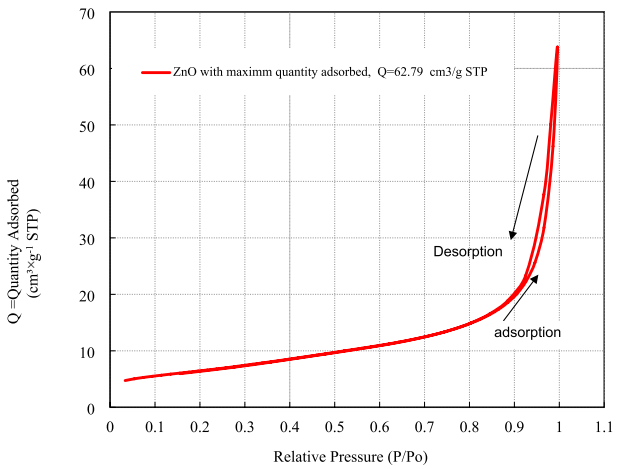

Fig. 7 Relation between relative pressure (P/P_o) and measured quantity adsorbed (Q) calculated by BET methods for ZnO nanoparticles

be independently determined using XRD and transmission electron microscopy (TEM) with the precision unavailable earlier. Density functional theory (DFT) methods have been first suggested by Lastoskie et al (1993) for calculating the pore size distribution of carbons from nitrogen adsorption data. The main advantages of the DFT methods are related to its rigorous theoretical basis that covers the whole region of micro- and mesopores and provides an opportunity of customization to different adsorbates (nitrogen, argon, and carbon dioxide), materials (silicas and carbons), and pore morphologies (slit-like, cylindrical, and spherical); the hybrid models that include different groups of pores were designed for hierarchical materials. Furthermore, the computational quantum mechanical modeling method, used in materials science, aids the investigation of adsorption structures and mechanisms of water adsorption on a high-index polar surface of ZnO. It provides explanations of not only the water adsorption behaviors of high index polar surfaces of ZnO but also guidance to all the adsorption behaviors of nanomaterial surfaces.

Effect of ZnO NP on IFT and contact angle

Different nanofluids were prepared by mixing ZnO NP at various concentrations (0.05, 0.075, 0.1) wt% with FW of different salinities. Figure 8 shows the IFT between the crude oil sample and the prepared nanofluids. It was found that as the concentration of NP increased the IFT of crude oil, and that of nanofluid decreased, where the minimum IFT value was obtained when using the nanofluid with the highest ZnO NP (0.1 wt%); these results agree with other reported results (Hendraningrat et al. 2013, 2012).

On the contrary, wettability measurements were obtained before and after surface modifications with different concentrations of NPs (0.05, 0.075, and 0.1 wt% ZnO) in FW

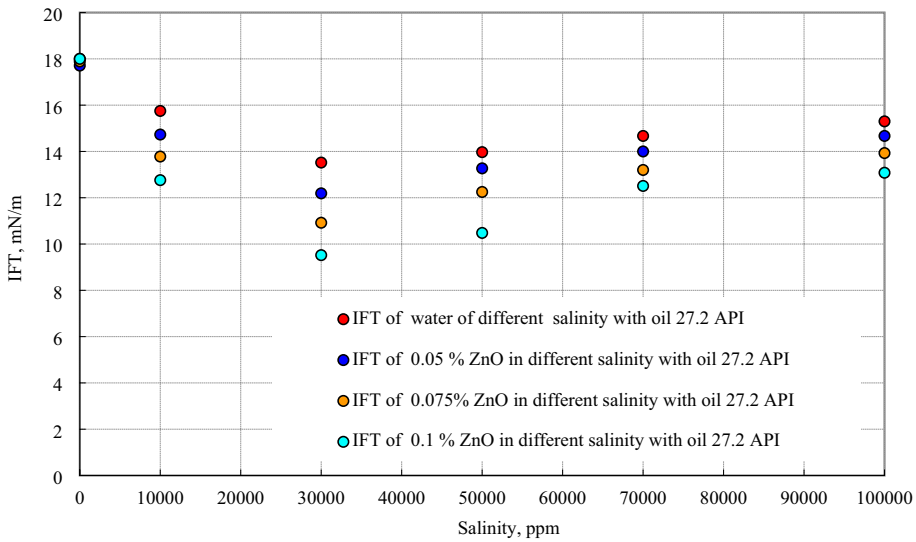

Fig. 8 Measured IFT between crude oil samples and different concentrations of ZnO NPs

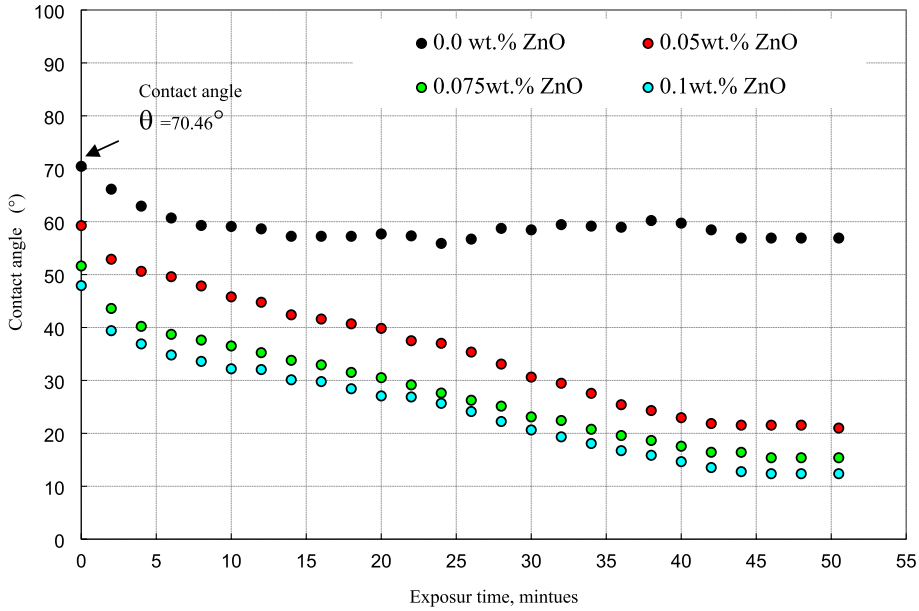

Fig. 9 Contact angles of rock-FW (30,000 ppm) and NP-oil systems

Table 6 Mass of rock core samples before and after LF-NMR measurements

Sample no	Experiment	Mass before (gm)	Mass after (gm)	Δ Mass (gm)
*S*0	Blank rock	27.9931	27.9758	0.0173
*S*1	Rock + FW	26.8585	26.5114	0.3471
*S*2	Rock + oil	27.7621	27.7276	0.0345
*S*3	Rock + oil + 0.5 PV nanofluid	28.8715	28.5500	0.3215
*S*4	Rock + oil + 1.0 PV nanofluid	28.0212	27.8348	0.1864
*S*5	Rock + oil + 1.5 PV nanofluid	27.4100	27.2314	0.1786
*S*6	Rock + oil + 2.0 PV nanofluid	26.7043	26.4966	0.2077

(30,000 ppm). The calculated values were obtained by analyzing the complete shape of the oil droplet using a precise video system and analysis software. Figure 9 shows that the surface immersed plates with and without nanoparticles. It could be seen that the value of dynamic contact angles for FW with no NP decrease at range (70.46–56.90°), with the drop value near to 19% of the original value, but for FW with NP at concentration range (0.05, 0.075, and 0.1) %, were (59.26–21.00°), (51.64–15.39°), and (47.92–12.3) respectively, indicating altered wettability in the water-wet condition. A stronger shift in wettability was achieved by increasing the NP concentration in the FW up to 0.075 wt% but small effect reaches the concentration 0.1 wt% (Fig. 9).

LF-NMR relaxometry

As stated earlier, the LF-NMR experiments were designed based on the results obtained through the IFT and contact angle measurements. Accordingly, 0.1 wt% ZnO nanofluid and 30,000 ppm of FW were used. Table 6 summarizes the details of the LF-NMR experiments conducted.

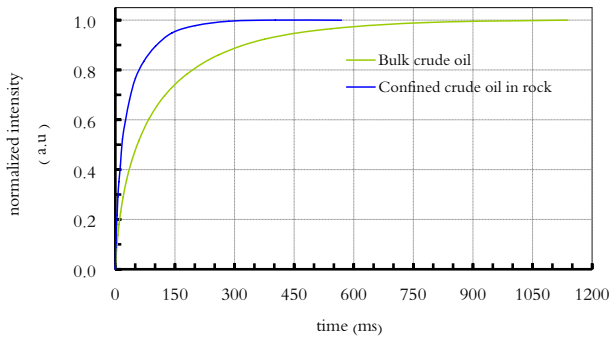

Fig. 10 Comparison of T_1 relaxation curves of bulk and confined crude oil (*S*2)

Dynamics of confined fluids

Figure 10 shows a representative comparison of the T_1 relaxation curves of bulk crude oil and confined crude oil (*S*2). As expected, the T_1 relaxation time of the confined crude oil (*S*2) shifted to lower values compared with that of the bulk crude oil. A similar, even stronger deviation in the T_1

Table 7 T_1 values of fluids in bulk and confined states

Case	$T_1(1)$ (ms)	$T_1(2)$ (ms)	$T_1(3)$ (ms)	$A_2(1)$ %	$A_2(2)$ %	$A_2(3)$ %
Bulk crude oil	202.7	49.9	7.6	50.3	35.7	14.0
Bulk FW	2649.0	–	–	100.0	–	–
*S*0	–	–	–	–	–	–
*S*1	105.3	16.6	3.3	20.0	58.9	21.1
*S*2	68.7	19.5	3.8	43.0	41.0	16.0
*S*3	66.4	18.7	4.0	36.4	39.4	24.2
*S*4	64.0	14.7	3.3	43.4	34.3	22.2
*S*5	68.7	16.3	3.3	38.0	41.0	21.0
*S*6	62.0	16.9	4.3	42.4	30.3	27.3

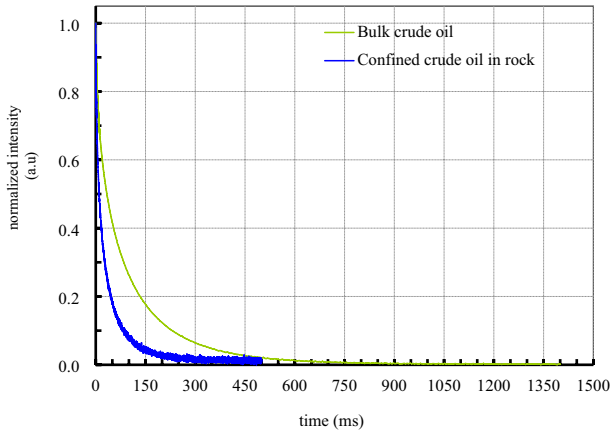

Fig. 11 Comparison of T_2 relaxation curves of bulk and confined crude oil (*S*2)

relaxation curve toward shorter times was observed in the case of FW (*S*1), as seen from Table 7. The T_1 values were determined using Eq. 1, based on three-component exponential growth fitting.

Figure 11 compares the T_2 relaxation curves of the bulk and confined crude oil (*S*2). As demonstrated in Table 7, the T_2 relaxation values of the confined crude oil (*S*2) are lower than those of the bulk crude oil. Additionally, compared with that of bulk FW, a stronger deviation in the T_2 relaxation curve with a shift toward shorter relaxation times was observed in confined FW (*S*1). This stronger deviation in FW is explained by the strong interaction between the water molecules and pore walls. The former preferably fill the smallest pores, and the surface relaxivity controls and reduces the T_2 value. Thus, the T_2 values of confined fluids are even lower than the corresponding T_1 values. Similarly, significant reductions in the relaxation times of the crude oil confined in rock samples compared with the bulk relaxation times offer evidence of surface relaxation (Freedman et al. 2003). A possible explanation is that when oil fills the larger pores, the ZnO NPs form an interphase (Myint et al. 2013; Soleimani et al. 2016), forming different types of environments: water in the smallest pores with the shortest relaxation, oil molecules in the larger pores, and mixed wettability, with water molecules wetting the pore walls, ZnO NPs between oil and water, and oil molecules not interacting directly with the pore walls. Table 8 summarizes the T_2 results, confirming that the deviations in the dynamic behaviors of the confined fluids from those of the bulk fluids are independent of NP treatment. The T_2 values are determined using Eq. 2, according to a three-component exponential decay fitting.

The first critical issue concerns the confinement effect on the dynamics of the fluids. Confinement in this case refers to "molecular confinement" where the crude oil and/or water molecules have spatial restrictions and different

Table 8 T_2 values of fluids in bulk and confined states

Case	$T_2(1)$ (ms)	$T_2(2)$ (ms)	$T_2(3)$ (ms)	$A_2(1)$ %	$A_2(2)$ %	$A_2(3)$ %
Bulk crude oil	160.5	47.8	7.1	44.1	36.6	19.4
Bulk FW	2173.0	–	–	100.0	–	–
*S*0	–	–	–	–	–	–
*S*1	89.4	15.8	1.9	15.8	44.7	39.5
*S*2	64.4	17.9	2.9	33.9	41.3	24.7
*S*3	53.1	14.0	2.9	27.7	42.2	30.1
*S*4	47.8	13.1	2.2	30.5	37.5	32.0
*S*5	55.1	14.7	2.7	27.6	39.2	33.1
*S*6	56.2	15.1	2.9	26.9	40.0	33.1

local chemical environment in the rock sample pores compared to that of bulk. In the confined geometry and environment, different properties such as dynamics of the molecules could differ from those in bulk. Independent of the chemistry, when the fluids (water or crude oil) were confined to sandstone, both T_1 and T_2 decreased. This shows that the confinement effect influences the wettability of the fluids with the grain walls. The second critical issue is the percentage of fluids in the bulk and confined states. Bulk FW has only a single value for both T_1 and T_2. However, the SARA (saturates, aromatics, resins, and asphaltenes) components of crude oil are considered with three different T_1 and T_2 values: longer, medium, and shorter. For the bulk crude oil, the lower $T_2(3)$ value of 7.1 ms constitutes 19.4% ($A_2(3)$), which corresponds to the heavy components (asphaltene + resins) of the crude oil. The larger $T_2(1)$ value of 160.5 ms constitutes 44.1% ($A_2(1)$) and is attributed to the lighter fractions (saturates) of the crude oil, as is also suggested in the literature (Volkov et al. 2021). The lighter fractions of the crude oil should thus have greater T_1 and T_2 values. Following the same approach, it is observed that in the confined state, crude oil has similar percentages of the different fractions under the different NP treatments.

T_1/T_2 ratios: affinity of fluids toward pore walls

To determine the affinity of the fluids toward the grain walls, the T_1/T_2 ratios were evaluated (Table 9) because the interactions between fluids and rock pores are reflected in the T_1/T_2 ratio. Moreover, being independent of pore geometry, these interactions are mainly influenced by the variations in surface relaxivity (Katika et al. 2017). Thus, the T_1/T_2 ratio is reliable for measuring the surface and bulk relaxations of fluids inside pores when the relaxations due to diffusion are negligible.

The most important result was observed in treatment with 0.1% ZnO NPs, which yielded a higher water wetting in the larger pores (Tinker 1983). Oil fractions interact weakly with the pore walls; hence, the oil-recovery efficiency is enhanced. For molecules such as simple liquids with fast anisotropic motion, T_1 and T_2 are equal, and hence, the ratio $T_1/T_2 = 1$ (Valori and Nicot 2018). For a molecule with slow dynamics, T_1 and T_2 differ and keep diverging further as the motion is hindered more. Second, the T_1/T_2 ratio for the oil may deviate from unity because of intrinsic bulk oil properties such as viscosity. Interpreting this deviation as the result of wettability might result in incorrect conclusions. A more reliable interpretation would be obtained by assessing the deviation from the unity of the water phase, which is expected to always have $T_1/T_2 = 1$ for the ideal non-wetting condition (Valori and Nicot 2018). As shown in Table 8, the $T_1(3)/T_2(3)$ values are similar in only FW-saturated and *S*4 (1.0 PV) samples. This shows that the treatment in S4 facilitates the pushing of the water molecules to the pore walls. In *S*3 (0.5 PV), the distribution of the fluids in the pores is mixed wetting. In other words, both FW and crude oil molecules could be found within the same porous regions.

Table 9 T_1/T_2 values of fluids in bulk and confined states

Case	$T_1(1)/T_2(1)$	$T_1(2)/T_2(2)$	$T_1(3)/T_2(3)$
Bulk crude oil	1.26	1.04	1.07
Bulk FW	1.22	–	–
*S*0	–	–	–
*S*1	1.18	1.05	1.74
*S*2	1.07	1.09	1.31
*S*3	1.25	1.34	1.31
*S*4	1.34	1.12	1.82
*S*5	1.25	1.11	1.22
*S*6	1.10	1.12	1.14

Wettability alteration

In this study, only T_1 distributions were used to analyze the wettability alteration potential by determining the porosity and permeability based on Eq. 3. Table 10 shows the NMR porosity, clay-bound water, and effective porosity (free fluid index) determined by analyzing the T_1 distributions obtained via inverse Laplace transform (ILT) of the T_1 relaxation data. Figure 12 shows the representative T_1 distributions of crude oil in the bulk and confined states for Berea sandstone (S2).

The total NMR porosity was 12.5% based on T_1, considering only the oil-flooded sample (*S*2). This value ensures suitable liquid characteristics before any NP treatment. The smaller pores resemble the clay-bound water porosity, which is approximately 0.20% based on the T_1 distribution analysis. The first saturation of the rock cores was with water, then with crude oil only, and finally with oil and nanofluid. The first saturation shows how water molecules behave in the smallest pores, while the second saturation (oil only) exhibits which pores the oil molecules wet. Based on these, we assign the shortest T_1, to water wet regions in the third wetting case. We use Eq. 3 to process the T_1 distribution data, and this helped obtain clay-bound water vs. free fluid index. Equation 3 does not require the use of T_1 cutoff value. In addition, processing T_1 distribution of *S*1 (only water wet sample) yields 0.2% for the smallest pores.

The completely water-wet pore size is best described as approximately 2.3% (0.29%/12.5%) of the total pore network. The effective porosity decreases when both FW and crude oil are used for flooding. Therefore, the effective porosity interphase should be a mixture of the oil + water region (between the clay-bound water and the free-oil region) and the free-oil zone. The effective porosity region is divided into two types: (1) bulk porosity-irreducible and

Table 10 Parameters determined by processing T_1 distribution data

Case	Total NMR porosity (p.u.)	Clay bound H_2O (p.u.)	Free fluid index (p.u.)	Clay bound H_2O/free fluid index (%)
*S*0	No signal	No signal	No signal	–
*S*1	0.76	0.20	0.45	44.4
*S*2	12.5	0.29	5.80	5.0
*S*3	11.1	0.43	4.40	9.8
*S*4	10.0	0.59	4.10	14.4
*S*5	10.1	0.45	4.10	11.0
*S*6	10.3	0.46	4.20	11.0

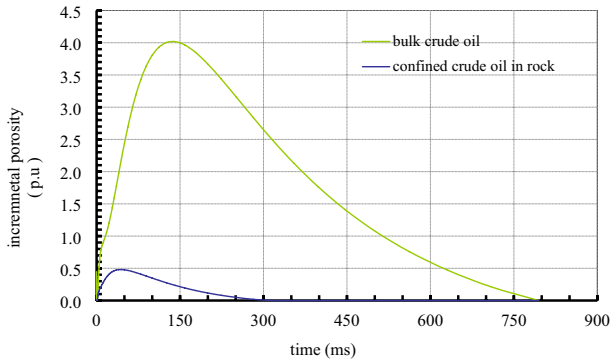

Fig. 12 Representative T_1 distributions of crude oil in bulk and confined states in Berea sandstone (*S*2)

(2) free fluid index. The first region is water dominant and has a transitional mixed zone of oil and water, while the second zone contains free crude oil. Water molecules wet the pore walls and simultaneously form an interphase with crude oil molecules. These observations pertain to two different wetting regimes: pore wall wetting and water–oil interphase wetting. In NP treated samples, the percentage of clay-bound H_2O/free fluid index was maximum in *S*4 with 1.0 PV NP treatment. This treatment should allow maximal crude oil recovery because the inner region of the sandstone with FW + NPs has the highest fraction and the affinity of crude oil molecules to interact with the pore walls of the sandstone was the lowest. Figure 13 demonstrates both T_1 and T_2 distribution comparison of the samples from *S*2 to *S*6. As expected, the time scale for T_1 distribution is longer than T_2 distribution. There was a shift, in both T_1 and T_2 distributions, to shorter times when ZnO NPs were utilized. The longer times in the distribution curves arise from larger pores with crude oil. T_1 and T_2 distribution curves of both *S*5 (1.5 PV) and *S*6 (2.0 PV) overlap each other, and longer times in their distributions resemble *S*2, oil only sample. In *S*3 (0.5 PV) and *S*4 (1.0 PV), the distribution curves differ from *S*2 (oil only), *S*5, and *S*6. Among the samples, *S*4 seem to be in between completely oil wet and completely mixed wetting. Therefore, *S*4 treatment with 1.0 PV, as also discussed above, will provide better wetting alteration and hence higher crude oil recovery.

ZnO NPs demonstrate a hydrophobic/hydrophilic switching ability depending on the treatment (Myint et al. 2013) as well as super-oleophilic properties (Jianlin et al. 2018). These NPs can be useful for establishing the interphase between water and crude oil molecules. Hence, crude oil molecules are segregated and do not wet the pore walls. The possible decrease in the surface energy of the water/ZnO NPs upon confinement in sandstone pores and upon interactions with the pore walls could lead to segregation of the crude oils.

Conclusion

This study was conducted to exhibit the potential of hydrophilic ZnO nanoparticles in enhance oil recovery by improving fluids–rock interaction properties such as wettability alteration. The nanoparticles are active on wettability alteration due to their ability to adsorption on or interact with the surface of the rock and altering the wettability from oil wet toward water wet. Interfacial tension measurements showed that ZnO NPs were able to reduce the FW-oil IFT from 18 to 9.52 mN/m depending on the ZnO NP concentration and FW salinity. The minimum IFT values were obtained at an optimal salinity of 30,000 ppm of FW with 0.1 wt% nanofluid. The effects of various concentrations of ZnO NP on wettability alterations, determined via contact angle measurements, indicated that depending on their concentration, the ZnO NPs were able to alter the wettability by changing the water–oil contact angle from 71° to 13°. When FW or crude oil was confined in the rock, deviations from their corresponding bulk dynamic behaviors were seen. This is attributed to the well-known confinement effect and is important because the NMR relaxation curves presented herein were acquired under confinement, where molecules have restricted motion. The percentage of clay-bound H_2O/free fluid index was the highest in *S*4 with 1.0

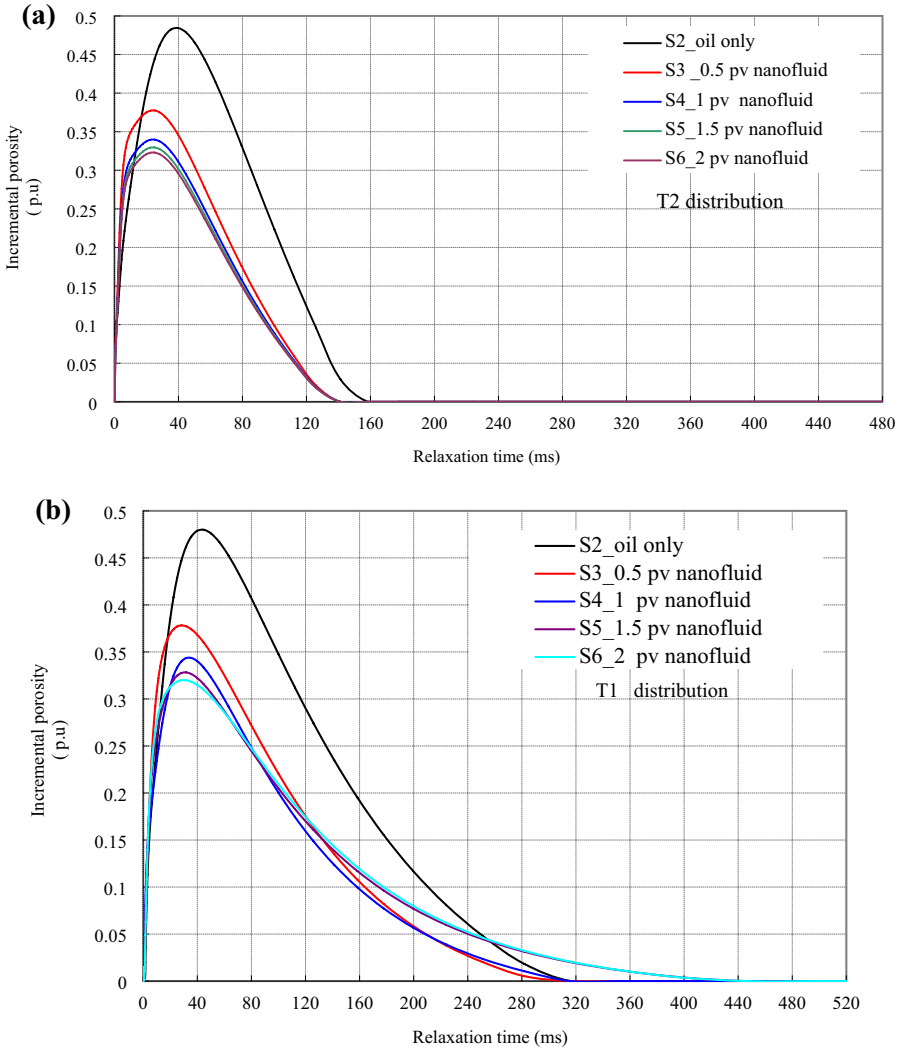

Fig. 13 T_2 (**a**) and T_1 (**b**) distributions of crude oils in confined states in Berea sandstone with and without utilization of ZnO NPs

PV NP treatment (for treated samples). The *S*4 treatment thus has a higher potential for wettability alteration under the confined state in porous rocks. A comparison of the T_1/T_2 ratio, an important parameter quantifying the affinity between the minerals and wetting fluid, also proved that the *S*4 treatment enables enhanced oil recovery because the $T_1(3)/T_2(3)$ values are similar in only FW-saturated and *S*4 (1.0 PV) NP-treated samples. Based on these results, it is possible to alter wettability using ZnO NPs under a confined geometry in rock samples for EOR studies. Furthermore, the LF-NMR method would be optimal for assessing the conditions for NP treatment in EOR. The potential of LF-NMR relaxometry was also demonstrated in water–oil interaction investigations with NP treatment at the subsurface of the rock matrix under a confined geometry. LF-NMR is therefore a promising technique for rock core analysis, petroleum chemistry, and behavioral studies of inorganic NPs in rock cores. Finally, the theories of porous-media relaxation support the applications of LF-NMR technologies.

Funding The authors are grateful for the help and support received from the Kuwait Foundation for the Advancement of Sciences (KFAS) (Research Grant PN1735EP01) and Kuwait University General Facility Research (GE 01/17–GS 01/01–GS 03/08–GS 01/05) for conducting the necessary experimental work. We are also grateful for the financial support by the Kuwait Institute for Scientific Research (KISR) in performing the LF-NMR measurements with Project Number PP066K.

Declaration

Conflict of interest The authors have no relevant financial or non-financial interests to disclose.

References

Abdallah W, Buckley JS, Carnegie A, Edwards J, Herod B, Fordham E, Graue A, Habashy T, Seleznev N, Signer C, Hussain H, Montaron B, Ziauddin M (2007) Fundamentals of wettability. Oil Field Rev 50:44–61

Abragam A (1961) Principles of nuclear magnetism. Clarendon Press, Oxford

Aghda SMF, Taslimi M, Fahimifar A (2018) Adjusting porosity and permeability estimation by nuclear magnetic resonance: a case study from a carbonate reservoir of south of Iran. J Petrol Explor Prod Technol 8:1113–1127. https://doi.org/10.1007/s13202-018-0474-z

Al Harbi AM, Gao J, Kwak HT, Abdel-Fattah AI (2017) The study of nanosurfactant EOR in carbonates by advanced NMR technique. SPE-188710-MS

Al-Anssari S, Barifcani A, Wang S, Maxim L, Iglauer S (2016) Wettability alteration of oil-wet carbonate by silica nanofluid. J Colloid Interface Sci 461:435–442

Ali JA, Kolo K, Manshad AK, Mohammadi AH (2018) Recent advances in application of nanotechnology in chemical enhanced oil recovery: effects of nanoparticles on wettability alteration, interfacial tension reduction, and flooding. Egypt J Pet 27:1371–1383

Almao PP (2012) In situ upgrading of bitumen and heavy oils via nanocatalysis. Can J Chem Eng 90:320–329

Alsaba MT, Al Dushaishi MF, Abbas AK (2020) A comprehensive review of nanoparticles applications in the oil and gas industry. J Pet Explor Prod Technol 10:1389–1399. https://doi.org/10.1007/s13202-019-00825-z

Alvarado RJ, Damgaard A, Hansen P, Raven M, Heidler R, Hoshun R, Kovats J, Morriss C, Rose D, Wendt W (2003) Nuclear magnetic resonance logging while drilling. Oil Field Rev 15(2):40–51

Anderson WG (1986) Wettability literature survey—part 2: wettability measurement. J Pet Technol 38:1246–1262

Aursand IG, Gallart-Jornet L, Erikson U, Axelson DE, Rustad T (2008) Water distribution in brine salted cod (*Gadus morhua*) and salmon (*Salmo salar*): a low-field ^{1}H NMR study. J Agric Food Chem 56:6252–6260

Ayatollahi S, Zerafat M (2012) Nanotechnology-assisted EOR techniques: new solutions to old challenges. Soc Pet Eng 157106094.

Azizr R, Joekar-Niasar V, Martinez-Ferrer P (2018) Pore-scale insights into transport and mixing in steady-state two-phase flow in porous media. Int J Multiphase Flow 109:51–62

Badalyan A, Pendleton P (2003) Analysis of uncertainties in manometric gas-adsorption measurements I: propagation of uncertainties in BET analyses. Langmuir 19:7919–7928

Barbosa LL, Kock FVC, Silva RC, Freitas JCC, Lacerda V Jr, Castro EVR (2013) Application of low-field NMR for the determination of physical properties of petroleum fractions. Energy Fuels 27:673–679

Barbosa LL, Kock FVC, Almeida VMDL, Menezes SMC, Castro EVR (2015) Low-field nuclear magnetic resonance for petroleum distillate characterization. Fuel Proc Technol 138:202–209

Barrett EP, Joyner LG, Halenda PP (1951) The determination of pore volume and area distributions in porous substances I computations from nitrogen isotherms. J Am Chem Soc 73(1):373–380. https://doi.org/10.1021/ja01145a126

Barroso AL, Marcelino CP, Leal AB, Odum DM, Lucena C, Masculo M, Castro F (2018) New generation nano technology drilling fluids application associated to geomechanic best practices: field trial record in Bahia, Brazil. In: Offshore technology conference, 30 April–3 May, Houston, Texas, USA. https://doi.org/10.4043/28731-MS

Bera A, Belhaj H (2016) Application of nanotechnology by means of nanoparticles and Nano dispersions in oil recovery—a comprehensive review. J Nat Gas Sci Eng 34:1284–1309

Borysenko A, Clenell B, Sedev R, Burgar I, Ralston J, Raven M, Dewhurst D, Lui K (2009) Application of low field and solid-state NMR spectroscopy to study the liquid/liquid interface in porous space of clay mineral and shales. Diffus Fund 10:21–24

Brunauer S, Emmett PH, Teller E (1938) Adsorption of gases in multi molecular layers. J Am Chem Soc 60:309–319

Brundle CR, Evans CA, Wilson S (1992) Encyclopedia of materials characterization: surfaces, interfaces, thin films. Gulf Professional Publishing, Houston

Cheraghian G, Hendraningrat L (2016) A review on applications of nanotechnology in the enhanced oil recovery part B: effects of nanoparticles on flooding. Int Nano Lett 6:1–10. https://doi.org/10.1007/s40089-015-0170-7

Cheraghian G, Rostami S, Afrand M (2020) Nanotechnology in enhanced oil recovery. Processes 8:1073. https://doi.org/10.3390/pr8091073

Chung SJ, Leonard JP, Nettleship I, Lee JK, Soong Y, Martello DV, Chyu MK (2009) Characterization of ZnO nanoparticle suspension in water: effectiveness of ultrasonic dispersion. Powder Technol 194:75–86

Connolly PRJ, Yan W, Zhang D, Mahmoud M, Verrall M, Lebedev M, Iglauer S, Metaxas PJ, May EF, Johns ML (2019) Simulation and experimental measurements of internal magnetic field. J Pet Sci Eng 175:985–997

D'Agostino C, Mitchell J, Gladden LF, Mantle MD (2012) Hydrogen bonding network disruption in mesoporous catalyst supports probed by PFG-NMR diffusometry and NMR relaxometry. J Phys Chem C 116:8975–8982

Dang CTQ, Nghiem LX, Chen ZJ, Nguyen QP (2013) Modeling low salinity waterflooding: ion exchange, geochemistry and wettability alteration. Soc Pet Eng. https://doi.org/10.2118/166447-MS

Dukhin AS, Goetz PJ (2010) Characterization of liquids, nano- and micro particulates and porous bodies using ultrasound, 2nd edn. Elsevier, p 24

Franco CA, Zabala R, Cortés FB (2017) Nanotechnology applied to the enhancement of oil and gas productivity and recovery of Colombian felds. J Pet Sci Eng 157:39–55. https://doi.org/10.1016/j.petrol.2017.07.004

Freedman R, Heaton N, Flaum M, Hirasaki GJ, Flaum C, Hurlimann M (2003) Wettability, saturation, and viscosity from NMR measurements. SPE J 87340:317–327

Gautam SS, Ok S, Cole DR (2017) Structure and dynamics of confined C–O–H fluids relevant to the subsurface: application of magnetic resonance, neutron scattering, and molecular dynamics simulations. Front Earth Sci 5:43-1-43–19

Giraldo J, Benjumea P, Lopera S, Cortes FB, Ruiz MA (2013) Wettability alteration of sandstone cores by alumina-based nanofluids. Energy Fuels 27:3659–3665

Gomez-Serrano V, Gonzalez-Garcia C, Gonzalez-Martin M (2001) Nitrogen adsorption isotherms on carbonaceous materials comparison of BET and Langmuir surface areas. Powder Technol 116:103–108

Gong L, Nie L, Xu Y (2020) Geometrical and topological analysis of pore space in sandstones based on X-ray computed tomography. Energies 13:3774. https://doi.org/10.3390/en13153774

Graves JE, Latvytė E, Greenwood A, Emekwuru NG (2019) Ultrasonic preparation, stability and hermal conductivity of a capped copper-methanol nanofuid. Ultrason Sonochem 55:25–31. https://doi.org/10.1016/j.ultsonch.2019.02.028

Gurgel A, Moura M, Dantas T, Neto EB, Neto AD (2008) A review on chemical flooding methods applied in enhanced oil recovery. Brazil J Pet Gas 2:83–95

Hashemi R, Nassar NN, Almao PP (2014) Nanoparticle technology for heavy oil in-situ upgrading and recovery enhancement: opportunities and challenges. Appl Energy 133:374–387

Hendraningrat L, Engeset B, Suwarno S, Torsater O (2012) Improved oil recovery by nanofluids flooding: an experimental study. In: SPE Kuwait international petroleum conference and exhibition. Soc Pet Eng. SPE-163335-1–SPE-163335-19

Hendraningrat L, Torsæter O, Li S (2013) Improved oil recovery by hydrophilic silica nanoparticles suspension: 2-phase flow experimental studies. In: International petroleum technology conference, Beijing, China, IPTC16707

Hoelscher KP, De Stefano G, Riley M, Young S (2012) Application of nanotechnology in drilling fluids In: SPE international oilfield nanotechnology conference exhibit, Noordwijk, The Netherlands, 12–14 June

Hou X, Zhu Y, Chen S, Wang Y, Liu Y (2020) Investigation on pore structure and multifractal of tight sandstone reservoirs in coal bearing strata using LF-NMR measurements. J Pet Sci Eng 187:106757

Hyne JB (1986) Aquathermolysis: a synopsis of work on the chemical reaction between water (steam) and heavy oil sands during simulated steam stimulation. Alberta Oil Sands Technology & Research Authority, Edmonton

Jiang J, Oberdörster G, Biswas P (2009) Characterization of size, surface charge, and agglomeration state of nanoparticle dispersions for toxicological studies. J Nano Res 11:77–89. https://doi.org/10.1007/s11051-008-9446-4

Jiang Y, Xu G, Hi H, Shi Y, Gao Y, Han X, Zeng X (2021) A new method to determine surface relaxivity of tight sandstone cores based on LF-NMR and high-speed centrifugation measurements. J Pet Sci Eng 196:108096-1-108096–9

Jianlin L, Xiaofei Z, Hongwei Z, Fuping W, Bigui W, Qing C (2018) Superhydrophobic coating on quartz sand filter media for oily wastewater filtration. Coll Surf A Physicochem Eng Aspects 553:509–514

Ju B, Fan T, Ma M (2006) Enhanced oil recovery by flooding with hydrophilic nanoparticles. China Particuol 4:41–46

Kanj MY, Rashid MH, Giannelis E (2011) Industry first field trial of reservoir nanoagents. In: SPE middle east oil and gas show and conference, 25–28 September, Manama, Bahrain. https://doi.org/10.2118/142592-MS

Katika K, Saidian M, Prasad M, Fabricius IL (2017) Low-field NMR spectrometry of chalk and argillaceous sandstones: rock-fluid affinity assessed from T_1/T_2 ratio. Petrophysics 58:126–140

Kazemzadeh Y, Shojaei S, Riazi M, Sharifi M (2019) Review on application of nanoparticles for EOR purposes: a critical review of the opportunities and challenges. Chin J Chem Eng 27:237–246

Kenyon WE, Kolleeny JA (1995) NMR surface relaxivity of calcite with adsorbed Mn^{2+}. J Colloid Interface Sci 170:502–514

Khalil M, Jan BM, Tong CW, Berawi MA (2017) Advanced nanomaterials in oil and gas industry: design, application, and challenges. Appl Energy 191:287–310

Khalilnezhad A, Rezvani H, Ganji P, Kazemzadeh Y (2019) A complete experimental study of oil/water interfacial properties in the presence of TiO_2 nanoparticles and different ions. Oil Gas Sci Technol Rev IFP Energies Nouvelles 74:39-1-39–14

Kokal S, Tang T, Schramm L, Sayegh S (1995) Electrokinetic and adsorption properties of asphaltenes. Colloids Surf A 94:253–265

Kondiparty K, Nikolov A, Wu S, Wasan D (2011) Wetting and spreading of nanofluids on solid surfaces driven by the structural disjoining pressure: statics analysis and experiments. Langmuir 27:3324–3335

Kosynkin D, Alaskar M (2016) Oil industry first inter-well trial of reservoir nanoagent tracers. In: SPE annual technical conference and exhibition, 26–28 September, Dubai, UAE. https://doi.org/10.2118/181551-MS

Lastoskie C, Gubbins KE, Quirke N (1993) Pore size distribution analysis of microporous carbons: a density functional theory approach. J Phys Chem 97(18):4786–4796

Lawson CL, Hanson RJ (1974) Solving least squares problems. Prentice-Hall Inc, Englewood Cliffs, p 158

Lianga C, Xiaoa L, Zhou C, Wang HC, Hu F, Lio G (2019) Wettability characterization of low-permeability reservoirs using nuclear magnetic resonance: an experimental study. J Pet Sci Eng 178:121–132

Maa C, Jin W, Ma X, Han H, Yu J, Wu Y (2019) Water adsorption behaviors of high index polar surfaces in ZnO. Appl Surf Sci 498(31):143898. https://doi.org/10.1016/j.apsusc.2019

Mirotchnik K, Kubika P, Randall L, Starosud A, Allsopp K, Kantzas A (1998) Determination of mud invasion characteristics of sandstone reservoirs using a combination of advanced core analysis techniques. In: International Symposium of the society of core analysts, Hague

Mirotchnik K, Kantzas A (1999) Methods and technology for the characterization of the pore structure and fluid flow properties of soils in reference to contaminant transport. J Can Pet Tech 38:41–47

Munson BR, Young DF, Okiishi TH (1998) Fundamentals of fluid mechanics, 3rd edn. Wiley, Hoboken

Murgich J (2002) Intermolecular forces in aggregates of asphaltenes and resins. Pet Sci Technol 20(9–10):983–997

Myint MTZ, Kumar NS, Hornyak GL, Dutta J (2013) Hydrophobic/hydrophilic switching on zinc oxide micro-textured surface. Appl Surf Sci 264:344–348

Nowrouzi I, Manshad AK, Mohammadi AH (2019) Effects of concentration and size of TiO_2 nanoparticles on the performance of smart water in wettability alteration and oil production under spontaneous imbibition. J Pet Sci Eng 183:106357-1-106357–14

Odusina EO, Sondergeld CH, Rai CS (2011) NMR study of shale wettability. Soc Pet Eng. https://doi.org/10.2118/147371-MS

Ok S, Mal T (2019) NMR spectroscopy analysis of asphaltenes. Energy Fuels 33:10391–10414. https://doi.org/10.1021/acs.energyfuels.9b02240

Olayiwola SO, Dejam M (2019) A comprehensive review on interaction of nanoparticles with low salinity water and surfactant for enhanced oil recovery in sandstone and carbonate reservoirs. Fuel 241:1045–1057

Onyekonwu MO, Ogolo NA (2010) Investigation the use of nanoparticles in enhancing oil recovery. Paper SPE 140744-Ms presented at Nigeria annual conference and exhibition, Tinapa-Calabar

Provencher SW (1982) A constrained regularization method for inverting data represented by linear algebraic or integral equations. Comput Phys Commun 27:213–227

Rahmani AR, Bryant S, Huh C, Athey A, Ahmadian M, Chen J, Wilt M (2015) Cross well magnetic sensing of superparamagnetic nanoparticles for subsurface applications. SPE J 20:1067–1082

Rezk MY, Allam NK (2019) Unveiling the synergistic effect of ZnO nanoparticles and surfactant colloids for enhanced oil recovery. Colloid Interface Sci Commun 29:33–39

Ridwan MG, Kamil MI, Sanmurjana M, Dehgati AM, Permadi P, Marhaendrajan T, Hakiki F (2020) Low salinity waterflooding:

Surface roughening and pore size alteration implications. J Pet Sci Eng 195:107868. https://doi.org/10.1016/j.petrol.2020.107868
Saien J, Gorji AM (2017) Simultaneous adsorption of CTAB surfactant and magnetite nanoparticles on the interfacial tension of n-hexane–water. J Molecule Liq 242:1027–1034
Siegbahn K, Nordling C, Fahlman A et al (1967) ESCA: atomic, molecular and solid state structure studied by means of electron spectroscopy. Almqvist & Wiksell International, Uppsala
Soleimani H, Yahya N, Baig MK, Khodapanah L, Sabet M, Bhat AH, Ochsner A, Awang M (2016) Catalytic effect of zinc oxide nanoparticles on oil-water interfacial tension. Dig J Nanometer Biostruct 11:263–269
Straley C, Rossini D, Vinegar H, Tutunjian P, Morriss C (1994) Core analysis by low field NMR. Soc Core Anal 4:43–56
Straley C, Morriss CE, Kenyon WE, Howard JJ (1991) NMR in partially saturated rocks: laboratory insights on free fluid index and comparison with borehole logs. Society petrophysicists well-log annual transactions SPWLA annual logging symposium, pp 1–25
Suleimanov BA, Ismailov FS, Veliyev EF (2011) Nanofluid for enhanced oil recovery. J Pet Sci Eng 78:431–437
Sulucarnain ID, Sondergeld CH, Rai CS (2012) An NMR study of shale wettability and effective surface relaxivity. In: SPE Canadian unconventional resources conference. society of petroleum engineers. https://doi.org/10.2118/162236-MS
Suryanarayana C, Mukhopadhyay D, Patankar S, Froes F (1992) Grain size effects in monocrystalline materials. J Mater Res 7:2114–2118
Teklu TW, Alameri W, Kazemi H, Graves RM (2015) Contact angle measurements on conventional and unconventional reservoir cores In: Proceedings of unconventional resources technology conference, San Antonio, USA
Tinker GE (1983) Design and operating factors that affect water flood performance in Michigan. J Pet Technol 35:1884–1892
Trevizan W, Coutinho B, Netto P, Rios E, Ramos P, Salazar J, Bressan M (2015) Magnetic resonance (NMR) approach for permeability estimation in carbonate rocks. In: Offshore technology conference, pp 1–12
Tso Ch, Zhung Ch, Shih Y, Tseng YM, Wu S, Doong R (2010) Stability of metal oxide nanoparticles in aqueous solutions. Water Sci Technol 61:127–133
Udoh TH (2021) Improved insight on the application of nanoparticles in enhanced oil recovery process. Sci Afr 13:e00873
Valori A, Nicot B (2018) A review of 60 years of NMR wettability. Soc Core Anal 17:1–13
Van SL, Chon BH (2016) Chemical flooding in heavy-oil reservoirs: from technical investigation to optimization using response surface methodology. Energies 9:711-1-711–19
Vogel M (2010) NMR studies on simple liquids in confinement. Eur Phys J Spec Top 189:47–64
Volkov VY, Al-Muntaser AA, Varfolomeev MA, Khasanova NM, Sakharov BV, Suwaid MA, Djimasbe R, Galeev RI, Nurgaliev DK (2021) Low-field NMR-relaxometry as fast and simple technique for in-situ determination of SARA-composition of crude oils. J Pet Sci Eng 196:107990
Wilson WW, Wade MM, Holman SC, Champlin FR (2001) Status of methods for assessing bacterial cell surface charge properties based on zeta potential measurements. J Microbiol Methods 43(3):153–164
Yahya N, Kashif M, Shafie A, Soleimani H, Zaid HM, Latiff NRA (2014) Improved oil recovery by high magnetic flux density subjected to iron oxide nanofluid. J Nano Res 26:89–99
Yoosuk B, Kim JH, Song C, Ngamcharussrivichai C, Prasassarakich P (2008) Highly active MoS2, CoMoS2 and NiMoS2 unsupported catalysts prepared by hydrothermal synthesis for hydrodesulfurization of 4,6-dimethyldibenzothiophene. Catal Today 130:14–23
Zabala R, Franco CA, Cortés FB (2016) Application of nanofluids for improving oil mobility in heavy oil and extra-heavy oil: a field test. In: SPE improved oil recovery conference, 11–13 April, Tulsa. https://doi.org/10.2118/179677-MS
Zaid HM, Yahya N, Latiff NRA (2013) The effect of nanoparticles crystallite size on the recovery efficiency in dielectric nanofluid flooding. J Nano Res 21:103–108
Zhang H, Nikolov A, Wasan D (2014) Enhanced oil recovery (EOR) using nanoparticle dispersions: underlying mechanism and imbibition experiments. Energy Fuels 28:3002–3009